

pubs.acs.org/JACS Article

Electrocatalytic Semihydrogenation of Terminal Alkynes Using Ligand-Based Transfer of Protons and Electrons

Maia E. Czaikowski, Sophie W. Anferov, Alex P. Tascher, and John S. Anderson*



Cite This: J. Am. Chem. Soc. 2024, 146, 476-486



Read Online

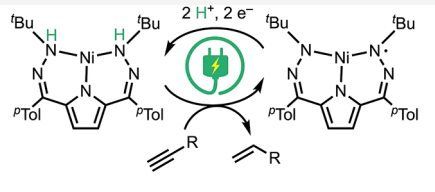
ACCESS I

III Metrics & More

Article Recommendations

s Supporting Information

ABSTRACT: Alkyne semihydrogenation is a broadly important transformation in chemical synthesis. Here, we introduce an electrochemical method for the selective semihydrogenation of terminal alkynes using a dihydrazonopyrrole Ni complex capable of storing an H_2 equivalent $(2H^+ + 2e^-)$ on the ligand backbone. This method is chemoselective for the semihydrogenation of terminal alkynes over internal alkynes or alkenes. Mechanistic studies reveal that the transformation is concerted and Z-selective. Calculations support a ligand-based hydrogen-atom transfer pathway instead of a hydride mechanism, which is commonly invoked for transition metal hydrogenation catalysts. The synthesis of the proposed intermediates demonstrates



Terminal alkyne selectivity
Ligand-based H⁺/e⁻ storage

Mechanistic study of hydride-free pathway

that the catalytic mechanism proceeds through a reduced formal Ni(I) species. The high yields for terminal alkene products without over-reduction or oligomerization are among the best reported for any homogeneous catalyst. Furthermore, the metal—ligand cooperative hydrogen transfer enabled with this system directs the efficient flow of H atom equivalents toward alkyne reduction rather than hydrogen evolution, providing a blueprint for applying similar strategies toward a wide range of electroreductive transformations.

■ INTRODUCTION

The semihydrogenation of alkynes is an important transformation in many pharmaceutical, agrochemical, and materials applications (Figure 1). $^{1-3}$ This importance has spurred a great deal of research into methodologies for the selective semihydrogenation of alkynes, with primary goals being the prevention of overreduction to alkanes as well as controlling E/Z selectivity. Lindlar's catalyst is a classic heterogeneous example that mediates the semihydrogenation of internal alkynes with Z selectivity. There have also been impressive advances with homogeneous catalysts for both E and Z-selective semihydrogenations, as well as recent advances in using more abundant first-row transition metal catalysts. $^{4-10}$

Despite these advances, there are several drawbacks to currently employed semihydrogenation technologies. Most methodologies typically operate under an $\rm H_2$ atmosphere which poses flammability and pressure hazards (Figure 1). Furthermore, selectivity against over-reduction to alkanes is typically dependent on steric changes upon conversion from an alkyne to an alkene. This manifests in a dearth of catalysts that are selective for the semihydrogenation of unprotected terminal alkynes without deleterious alkyne dimerization, overreduction, or catalyst decomposition. 11,12 These challenges motivate the discovery of new alkyne semihydrogenation processes.

In thinking of alternative semihydrogenation protocols, and particularly in strategies that avoid the use of gaseous H_2 , electrochemical transformations have many innate benefits. Electrocatalysis allows for precisely controlled redox transformations without the addition of stoichiometric chemical

reductants or oxidants.^{13–16} The direct synthetic use of electricity can also provide a sustainable methodology when electricity is sourced renewably. These factors, coupled with the decreasing cost of renewable electricity, motivate investigations into converting classic thermal industrial and fine chemical transformations into electrocatalytic processes.¹⁷ These attractive features have made electrocatalytic reductive transformations a burgeoning area, but homogeneous electrocatalysts are comparatively under-explored for these useful reactions.^{18–28}

For alkyne semihydrogenation in particular, two electrocatalytic Ni and Co bipyridine complexes have shown good efficiency with internal alkynes with good to excellent Z selectivity. However, both of these systems suffer from poor tolerance of terminal alkyne substrates, attributed to the propensity for dimerization and overreduction. Recent mechanistic investigations of the Ni bipyridine electrocatalytic system suggest a hydride-free mechanism for this transformation, which is in contrast to the prevailing mechanism for most homogeneous semihydrogenation catalysts involving the formation of a metal hydride which engages in alkyne

Received: September 8, 2023 Revised: December 13, 2023 Accepted: December 14, 2023 Published: January 1, 2024





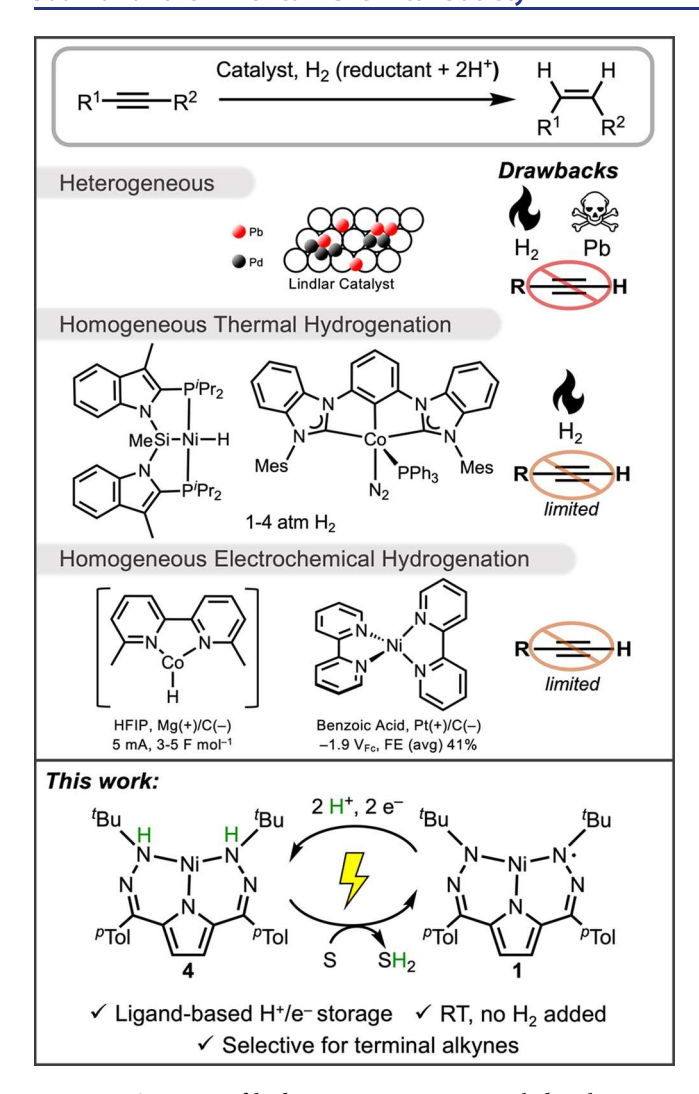


Figure 1. Overview of hydrogenation strategies, including heterogeneous, homogeneous, and electrochemical systems.

reduction.³¹ In either mechanistic scenario, the controlled flow of H atom equivalents is critical to turnover and selectivity.

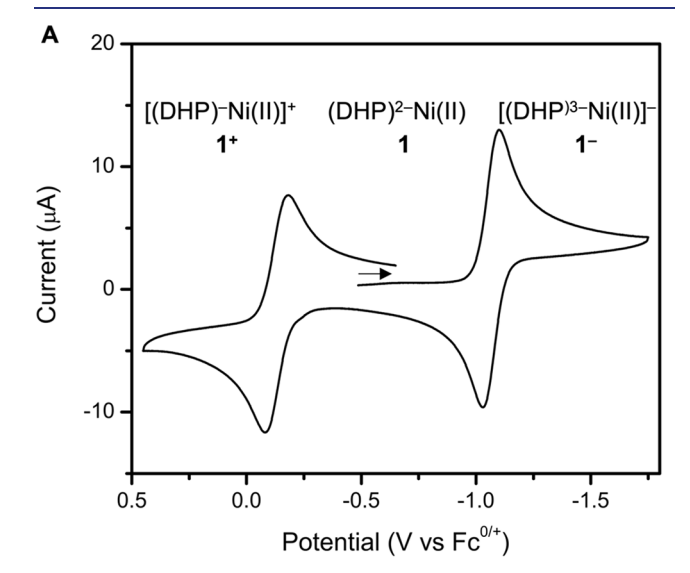
We have been interested in utilizing ligand-based storage of H_2 , or equivalently H^+ and e^- equivalents, to mediate both reductive and oxidative transformations. This approach relies on the storage and transfer of H atom equivalents from the ligand, akin to enzymatic systems, thus enabling new strategies for achieving challenging and novel transformations. While several systems have demonstrated H atom storage, examples of the ligand-based storage of a full equivalent of H_2 are more uncommon. We have specifically been investigating a dihydrazonopyrrole (DHP) ligand scaffold that can store a full equivalent of H_2 which enables catalytic thermal hydrogenations of alkenes and quinones. Given this reactivity, we questioned whether H_2 could be replaced by acid and an electrode and also whether the metal—ligand cooperative hydrogenation reactivity and selectivity of this system would be altered under this electrochemical regime.

Indeed, we have found that DHP Ni complexes are excellent electrocatalysts for the selective semihydrogenation of alkynes (Figure 1). Specifically, we see good selectivity and conversion with a broad scope of alkynes, particularly terminal alkynes, without evidence of over-reduction or oligomerization. Mechanistic investigations underscore the importance of the

DHP ligand stored reducing equivalents, in parallel to recent observations of hydride-free mechanisms. Finally, this system displays good efficacy and scope for a variety of substrates, including drug molecules and diynes. These results add to the growing body of literature demonstrating the utility of reductive electrocatalysis in providing alternative strategies to classic transformations and also demonstrate how metalligand cooperative strategies for H_2 or H_2 atom storage can enable new catalysis.

RESULTS AND DISCUSSION

Electrochemical Characterization. We initially targeted the previously reported complex ($^{\mathrm{Bu,Tol}}\mathrm{DHP}$)Ni(II) (1) as a precatalyst. The cyclic voltammogram (CV) of 1 in acetonitrile shows two reversible redox events at peak potentials ($E_{1/2}$) of -0.1 and -1.1 V vs $\mathrm{Fc}^{0/+}$. We assign these features to ligand-based oxidation and reduction of the starting complex to form 1^+ and 1^- , respectively (Figure 2A). Additionally, the CV of 1 in THF possesses a quasi-reversible



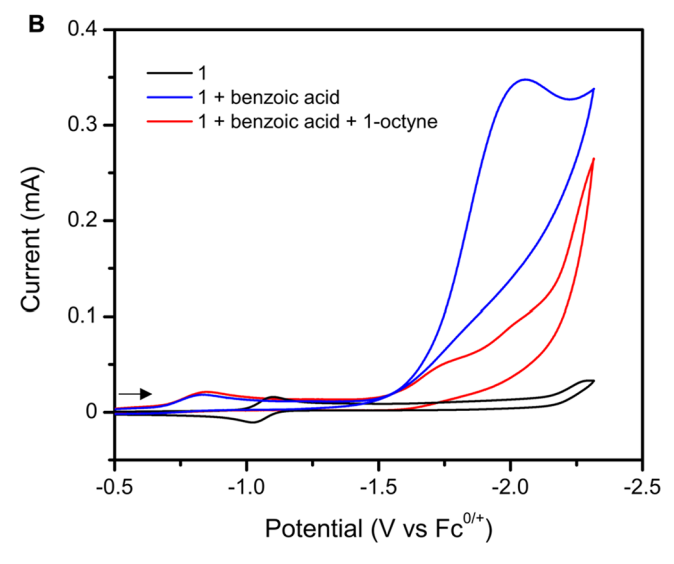


Figure 2. (A) CV of 1 (1 mM) in MeCN. 0.1 M TBAPF $_6$, 100 mV s⁻¹, scanning reductively. (B) CV of 1 alone, with 10 eq benzoic acid, and with 10 eq benzoic acid and 10 eq 1-octyne. One mM 1, 0.1 M TBAPF $_6$ in MeCN, 100 mV s⁻¹, scanning reductively.

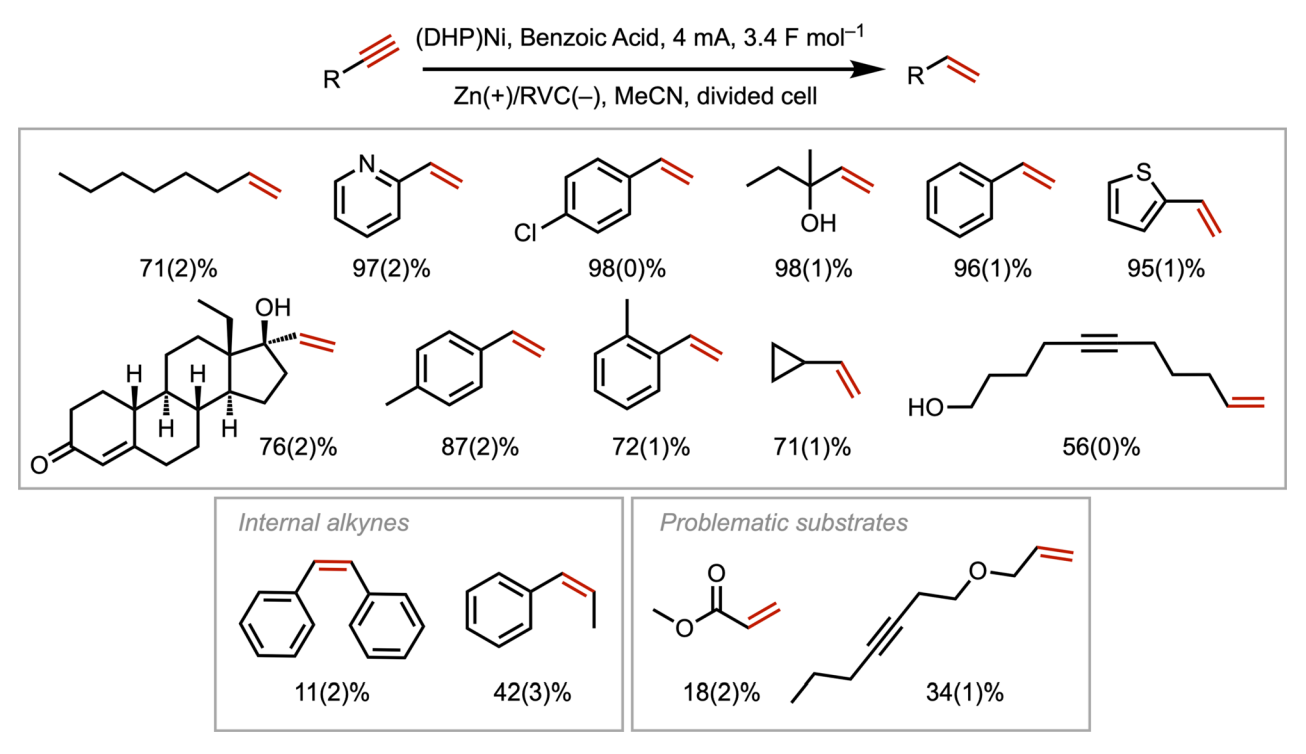


Figure 3. Substrate scope for alkyne semihydrogenation using 1 mM 1, 10 mM substrate, and 100 mM benzoic acid in MeCN. 0.1 M TBAPF₆, constant current electrolysis, t = 55 min. In situ chemical yields are given as a percentage with standard deviation in parentheses. F mol⁻¹ calculated based on alkene under galvanostatic conditions at 4 mA.

reduction at -2.6 V vs $Fc^{0/+}$ which we assign to a putative Ni(II)/(I) couple (Figure S13). To test the possibility of electrochemical hydrogenation with 1, we initially investigated how these CV features were affected by the added acid. These experiments are particularly important, as parasitic H_2 evolution is likely to be competitive with any desired hydrogenation reactivity.

The first reduction feature of 1 shifts 300 mV anodically and becomes irreversible upon the addition of 10 equiv of benzoic acid, likely due to protonation of the ligand altering the reversibility of this reduction (Figure 2B). Complex 1 also displays an electrocatalytic onset at $-1.5~\rm V$ vs Fc $^{0/+}$ in the presence of benzoic acid. This onset is 500 mV less negative than the onset potential of benzoic acid on the carbon electrode surface alone. This catalytic response is due to $\rm H_2$ evolution and we note that many Ni catalysts are known to be active electrocatalysts for this reaction (Figure S60).

Despite the potential for H_2 evolution side reactivity, we still wanted to test whether the net H^+ and e^- equivalents delivered electrochemically could be harnessed for hydrogenation reactivity. Indeed, upon the addition of 1-octyne, the catalytic feature at -1.5~V vs $Fc^{0/+}$ is suppressed and adopts a new waveform consistent with a change in reactivity in the presence of an alkyne substrate (Figure 2B). This suggests that the catalytically active form of 1 may selectively react with an alkyne substrate despite competing hydrogen evolution reactivity (HER). These promising initial results from CV prompted us to perform bulk electrolyses to determine the major product of alkyne reactivity and whether this catalytic system diverts H atom equivalents from HER efficiently.

Semihydrogenation Reactivity and Scope. Bulk electrolysis was carried out under a constant current in a divided cell. Under standard conditions ([Ni] = 1 mM; [alkyne] = 10 mM; [BA] = 100 mM; i = 4 mA, t = 55 min),

terminal alkyne substrates were successfully semihydrogenated and overreduced or oligomerized byproducts were not detected by GC/MS analysis. The semihydrogenated product of 1-octyne is produced in 71% chemical yield and 33% Faradaic efficiency (FE). The conversion of phenylacetylene to styrene proceeds in 96% chemical yield with a 45% FE. While the yield and FE for aliphatic terminal alkynes are somewhat lower than those for phenylacetylenes, the observed conversion and yields here are among the best reported across both aryl and alkyl terminal alkynes in any homogeneous catalytic system. Control electrolyses excluding 1 or benzoic acid showed no conversion of the 1-octyne starting material. Substituting 1 with a generic Ni salt, Ni(MeCN)₃OTf₂, resulted in a mixture of 1-octene and oligomeric products in 11 and 14% yield, respectively (Figure S62). This loss of selectivity and conversion for semihydrogenation with a generic Ni salt is reminiscent of the lower yields and conversion for many other catalysts for the reduction of terminal alkyne substrates, indicating an essential role for the dihydrazonopyrrole ligand in the high selectivity we observe. As a final control, postelectrolysis electrodes are inactive in fresh electrolyte without 1. Together, these tests strongly support the idea that the active catalyst species involves a welldefined molecular (fBu,TolDHP)Ni complex.

Various parameters were tuned to optimize the conditions for bulk electrolysis and maximize the yield of semi-hydrogenated products. Modifying the current showed that 4 mA produced an optimal yield with again a surprisingly good FE of 40–50% for most substrates (Table S1). Using hexafluoroisopropanol as a proton source resulted in poor yields, as did switching to the THF solvent. The maximum yield and FE were achieved at 55 min of constant current with plateauing yields with further time (Figure S19). An RVC electrode was selected to disfavor HER, and yields improved

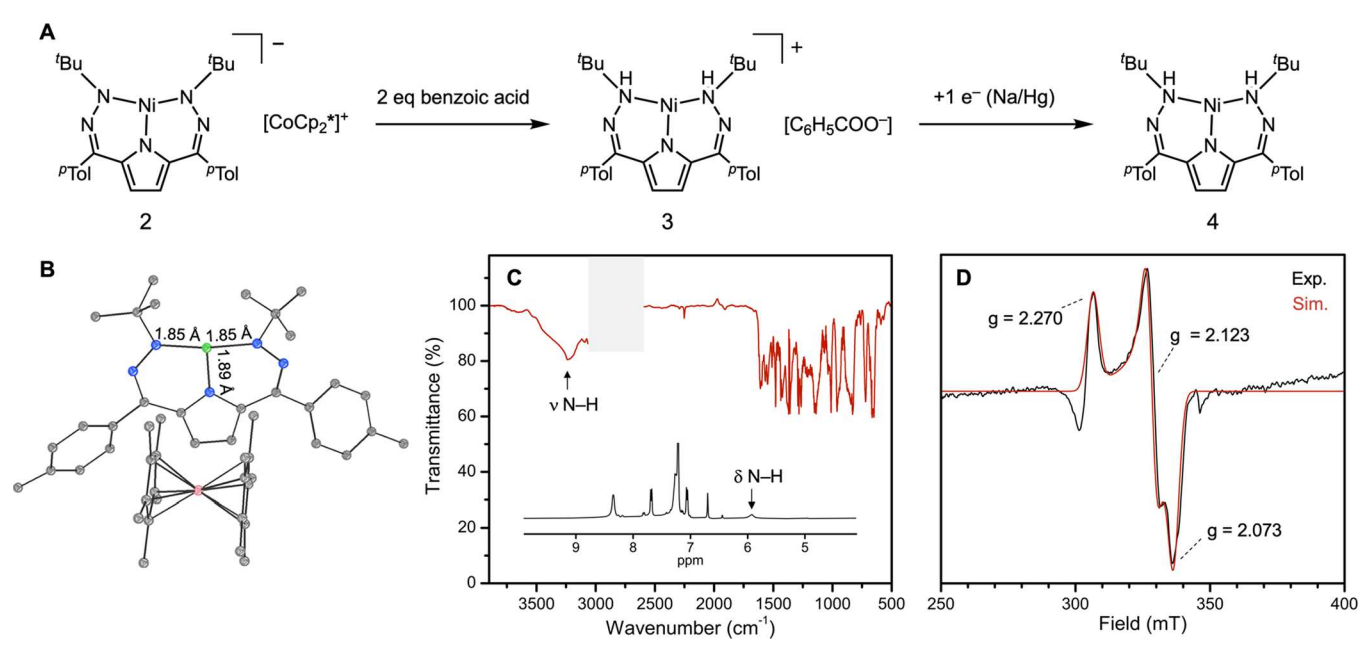


Figure 4. (A) Synthesis of in situ (1Bu,Tol DHP)Ni intermediates (B) SXRD structure of **2**. Ellipsoids are set to the 50% probability. Hydrogen atoms have been omitted for clarity. (C) IR in THF and NMR (inset, in C_6D_6/d_8 -THF) spectra of **3** in showing the N–H stretching feature and chemical shift, respectively. Imperfect solvent subtraction is removed from the IR spectrum for clarity. (D) X-band EPR spectrum of **4** in MeCN at 15 K. We note the small paramagnetic impurities at 300 and 345 mT; see Figure S23 for the full spectrum.

by 10-20% compared to a graphite rod electrode.⁷² Optimized electrolyses were performed in a divided cell. While conversion also proceeds in good yield with an undivided cell, Zn^0 plating from the sacrificial Zn anode onto the RVC cathode was avoided in a divided cell.

A variety of substrates were then tested under these optimized conditions to determine the reaction scope. A broad set of functional groups were tolerated including pyridines, thiophenes, aryl chlorides, cyclopropyl, and hydroxyl groups (Figure 3). Good yields of the corresponding terminal alkene were also observed for the common drug compound levonorgestrel, which possesses a tertiary alcohol group as well as an $\alpha_{i}\beta$ -unsaturated carbonyl. This result supports the ability of 1 to perform late-stage semihydrogenations of terminal alkynes in complicated molecules. Furthermore, 3.4 F mol⁻¹ is passed in all cases, consistent with near 50% FE for semihydrogenation over hydrogen evolution for most substrates. The functional group tolerance of 1 is improved in comparison to recent Ni electrocatalysts³⁰ and is similar to recent Co systems, ²⁹ with the notable exception of ester groups which are not well-tolerated in our case. We note that the activity of 1 for unprotected terminal alkynes is unusual for homogeneous electrocatalytic systems, with only limited activity or selectivity as shown in previous reports.

We can also compare the activity of 1 to the limited examples of terminal alkyne thermal semihydrogenations using H₂. Complex 1 has an improved scope and yield over a previously reported Mn bis(di-iso-propylphosphino)ethane catalyst, and comparable tolerance of chlorides, thiophenes, and methyl-substituted phenylacetylenes to a Fe N-methyl PNP pincer catalyst. We note the observation that improving the bulkiness of the PNP pincer ligand for the aforementioned Fe catalyst improved selectivity for the semihydrogenated terminal alkene product rather than dimerized or overreduced byproducts. Likewise, in our system, we hypothesize that the bulkiness of the tBu groups around the Ni center introduces

steric hindrance that selects terminal alkyne substrates over alkenes or bulkier internal alkynes. This is exemplified by the 11% yield of stilbene obtained from diphenylacetylene with 1 under the standard electrolysis conditions, with the remainder of the carbon balance corresponding to the unreacted starting material.

Catalytic Mechanism. The high activity and selectivity of 1 motivated us to investigate its mechanism. An important mechanistic question is whether 1 directly reduces alkynes, or whether in situ-generated H_2 enables thermal hydrogenation catalysis. However, electrolysis of 1 and 1-octyne with an atmosphere of H_2 results in <5% yield of 1-octene (Table S1). This demonstrates that any H_2 generated during electrocatalysis contributes only minimally to product formation. This finding is consistent with previous studies which showed this system is capable of activating H_2 for quinone hydrogenation, but not for alkenes. ⁵⁸

The order in benzoic acid for semihydrogenation cannot be concretely determined by analyzing the CV due to overlapping HER (Figure 2). However, we note that the initial feature of the catalytic wave only appears when the substrate is present along with acid and that increasing benzoic acid concentration does not increase the current of this feature (Figure S17). These observations suggest that catalytic turnover is zero order in acid, which is supported by the DFT-calculated rate-determining step of intramolecular HAT (vide infra). The addition of 1-octyne suppresses the HER wave of 1 but increasing the 1-octyne concentration beyond an equimolar amount with benzoic acid does not provide any further change in the catalytic wave (Figure S15).

We then analyzed the speciation of 1 with added acid or substrate by CV. The addition of 1-octyne to 1 without any added acid shows no change in the reversible redox features, suggesting that 1 does not bind 1-octyne in its neutral or 1⁻ reduced oxidation state (Figure S14). The addition of substoichiometric benzoic acid to 1 without added 1-octyne

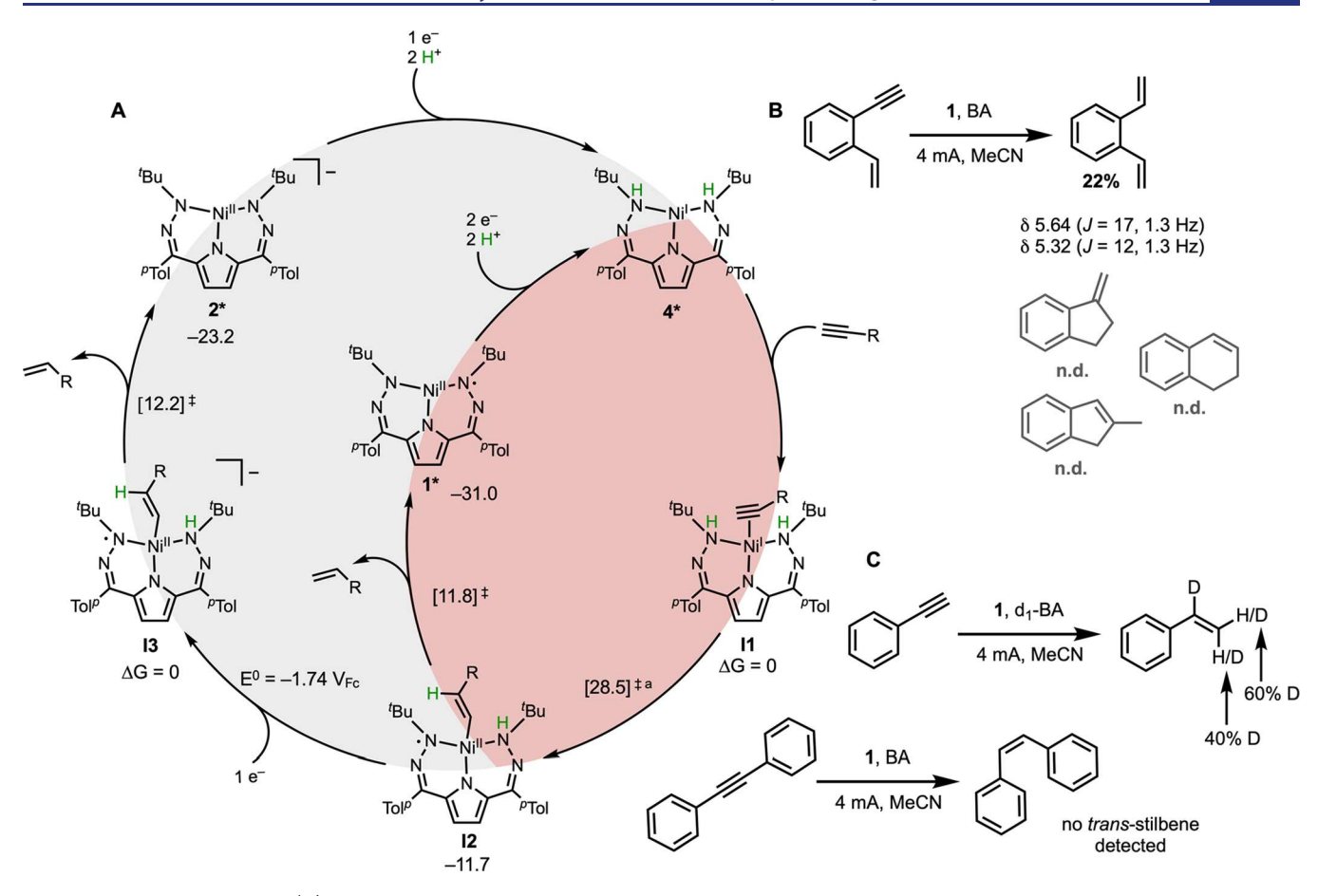


Figure 5. Mechanistic studies. (A) Proposed catalytic cycle with neutral and anionic pathways shown. ^aThis TS1 energy is an upper-limit from the most reasonable TS1 geometry obtained but is not fully optimized (see SI, Figures S66 and S75). DFT computed energies (kcal/mol) were carried out with the M06L functional, def2-TZVPP basis set for Ni, and def2-TZVP for all other atoms. Asterisks indicate experimentally characterized intermediates. We note that TS1 between I1 and I2 has an elongated Ni–N5 distance (Figure S66). Shown oxidation states are only formalisms, and the redox-active nature of the DHP scaffolds convolutes concrete oxidation state assignments. (B) Radical probe experiment using allyl-2-ethynylbenzene and (C) deuterium incorporation experiment using d_1 -benzoic acid with phenylacetylene, and semi-hydrogenation of diphenylacetylene to give 11% chemical yield of *cis*-stilbene with no *trans* product detected. Standard electrolysis conditions: [Ni] = 1 mM; [alkyne] = 10 mM; [BA] = 100 mM; [TBAPF₆] = 0.1 M; i = 4 mA, t = 55 min, MeCN, RVC/Zn.

induces a color change from deep purple to maroon and improved solubility in MeCN compared to the starting complex. The CV of this mixture shows a gradual diminishment of the reversible redox feature at $-1.1~\rm V$ vs $\rm Fc^{0/+}$ as two new irreversible features arise at $-0.6~\rm and~-0.9~\rm V$ vs $\rm Fc^{0/+}$ (Figure S16). Eventually, the dominant feature is a broad irreversible reduction at $-0.9~\rm V$ vs $\rm Fc^{0/+}$ after >2 equiv of benzoic acid has been added (Figure S17). We postulate that the speciation at low concentrations of acid arises from an equilibrium between mono- and diprotonated analogues of 1. The single irreversible feature with additional acid possibly corresponds to the reduction of a diprotonated ligand—metal complex. However, a more detailed assignment of differentially protonated congeners of 1 is challenging due to the paramagnetic nature of these species.

While the product(s) of 1 and benzoic acid are paramagnetic and difficult to characterize, the initial reduction of 1 with 1 eq of $CoCp_2*$ provides $[(^{fBu,Tol}DHP)Ni]^-[CoCp_2*]^+$ (2) which is diamagnetic (Figure 4B). This enables protonation studies with NMR spectroscopy, and the addition of 2 equiv of benzoic acid to 2 results in a color change from indigo to light yellow. We tentatively assign this new product as $[(^{fBu,Tol}DHPH_2)Ni]^+[BzO]^-$ (3) where the β -Ns of both

hydrazone arms have been protonated. Evidence of these protonated ligand arms is provided by ^1H NMR ($\beta\text{-NHs}\colon 5.92$ ppm) and IR (N–H: 3250 cm $^{-1}$) spectroscopies which show diagnostic resonances and stretches, respectively (Figure 4C). Furthermore, the ^1H NMR of 3 is in agreement with the previously reported and characterized complex ($^{\text{fBu,Tol}}\text{DHPH}_2$)NiOTf. 58

Interestingly, no hydrogenated products are observed when 3 is stirred with excess 1-octyne. This indicates that 3 is not an active hydrogenating intermediate. The catalytic CVs for 1 support this hypothesis. The onset potential for catalysis begins at nearly 0.7 V negative of the first irreversible reduction of the Ni complex in the presence of benzoic acid. We hypothesized that an additional reduction event corresponding to a formal Ni(II)/Ni(I) couple might be necessary for catalysis. Indeed, isolated (fBu,TolDHPH2)NiOTf has an irreversible reduction feature at -1.6 V vs $\text{Fc}^{0/+}$, which is nearly superimposable with the catalytic onset of 1 in the presence of benzoic acid (Figure S21). As this complex has a reduced DHP ligand, this feature is most reasonably assigned as a Ni(II)/Ni(I) couple. The irreversibility of this feature is likely induced by a chemical change, such as proton loss upon reduction. While 3 is not reactive with 1-octyne, the addition of Na amalgam as a

reductant with 3 leads to the production of 1-octene in 27% yield (Figure S6). We attribute this comparatively low yield to some decomposition of complex 3 owing to the strongly reducing conditions. Stirring 1-octyne and benzoic acid with Na/Hg in the absence of 3 recovers only the 1-octyne starting material. To further corroborate the presence of a Ni(I) species, compound 3 was stirred with Na/Hg followed by rapid freezing at $-78~^{\circ}$ C. The X-band EPR spectrum is consistent with a Ni(I) species, with a broad rhombic signal and features at g=2.073, 2.123, and 2.270 (Figure 4D). The EPR spectrum is distinct from that of complex 1 which is formally Ni(II) with a ligand radical. These combined data, and particularly the need to add an additional reductant to 3 to react with alkynes, supports that a reduction to a Ni(I) species (4) is critical to initiating catalysis.

With evidence supporting the necessity of the two-electron reduction of 1 in the presence of acid before the system is catalytically active, we then investigated the chronoamperometry of bulk electrolyses to gain additional mechanistic insights. Specifically, we noted a distinctive initiation period that we thought might correspond to an initial reduction of the Ni species in solution (Figure S19). Calculating the moles of electrons passed during this period corresponds with a two-electron reduction of the added catalyst (see SI). Use of (fBu,TolDHPH2)NiOTf instead of 1 should in principle reduce this induction period as the catalyst is already reduced. Satisfyingly, this substitution indeed shortens the initiation period and reaches a similar potential and overall yield as the standard conditions, which supports the hypothesis that a Ni(I) species needs to be generated (Figure S20).

We also wanted to obtain more insight into the net H atom transfer steps of catalysis, so we analyzed the products of the low-yielding internal alkyne substrates diphenylacetylene and 1-phenyl-1-propyne. We found that both of these substrates gave the Z-isomer of the stilbene and β -methyl-styrene products, respectively (Figures S49 and S50). While no E products were detected for these internal alkyne substrates, deuterium labeling studies with d_1 -benzoic acid and phenylacetylene revealed a 1:0.6 Z:E ratio for terminal alkyne semihydrogenation (Figure SC). These observations suggest that the semihydrogenation proceeds in a cis-selective manner with some possible competition or isomerization for terminal alkyne substrates. It is possible that the smaller steric profile of terminal alkene products might favor coordination to Ni and subsequent isomerization.

As a last mechanistic test, we also investigated the possible involvement of radical intermediates, such as free alkenyl radicals. We note that previous thermal hydrogenations with DHP complexes of Co do show evidence for radical intermediates.³² To test this possibility, we employed a radical cyclization probe, allyl-2-ethynylbenzene, which might be expected to undergo cyclization to a five-membered ring from a putative radical intermediate (Figure 5B). While this compound is unstable and undergoes some degree of polymerization in MeCN, we detected no cyclized products and solely the expected 1,2-divinylbenzene product which should arise from hydrogenation (Figure S10). The rate constant for cyclization for similar vinyl radical species is on the order of 10⁸ s⁻¹, indicating that semihydrogenation proceeds through a concerted mechanism without long-lived radical intermediates.7

We then employed density functional theory (DFT) computations to gain additional mechanistic insight and to

fill in a complete mechanistic cycle (Figure 5A). Beginning from fully reduced Ni(I) complex 4, coordination to 1-butyne gives calculated bond distances of 1.969 and 2.008 Å, showing a nearly symmetrically bound alkyne. The first net H atom transfer (HAT) has an estimated upper limit transition state barrier of 28.5 kcal/mol (TS1, see below and SI for further discussion, Figures S66 and S75) and is overall exergonic by 11.7 kcal/mol. After this initial step to form I2, we envisioned two plausible pathways by which the cycle could proceed. A second HAT could release the alkene product and give 1. This path proceeds via a ~23 kcal/mol transition state barrier (TS2, Figure S71) for an overall 19 kcal/mol downhill process. If instead the alkenyl adduct is first reduced by one electron to generate I3, the subsequent transition state barrier for HAT is 12.2 kcal/mol (TS2-, Figure S69) for an overall 23.2 exergonic process. Both pathways regenerate starting species 4 by subsequent reduction and protonation. DFT calculations predict that TS1 represents the rate-determining step, however, we have had difficulties obtaining a reliable geometry and energy for this TS (see experimental and SI, Figures S66 and \$75). Furthermore, the comparable energy between TS1 (28.5 kcal/mol) and TS2 (23.5 kcal/mol) makes drawing concrete conclusions about the rate-determining step difficult. The low transition state barrier for the second HAT step, along with the accessible calculated reduction potential of $-1.74~\mathrm{V}$ vs $Fc^{0/+}$ in MeCN, supports the idea that reduction to an anionic alkenyl intermediate I3 is at least a plausible cycle.

One interesting feature of this proposed cycle is the lack of any metal-hydride intermediates. To further test this observation, we computationally explored the feasibility of a Ni hydride species via the reduction and migration of one proton from the ligand. The formation of a (DHP)Ni-H species is calculated to be slightly endergonic, and the resultant coordinatively saturated hydride species is not computed to have favorable alkyne binding (Tables S16 and S17). We also note that we have seen no evidence by either ¹H NMR or IR spectroscopy that would indicate the presence of a hydride species, but we do observe ligand-based proton storage for 3 which is the precursor to the proposed catalytically active complex 4 (Figures S3 and S24). These data suggest that the ligand-based reactivity is the most viable pathway. This hydride-free pathway echoes recent mechanistic proposals from Leitner and co-workers where an ECEC semihydrogenation pathway with a nickelacyclopropene adduct resting state was invoked.³¹ This system uses a bipyridine ligand and relies on direct outer sphere protonation to a reduced metallacyclopropene intermediate followed by rapid electron transfer. In contrast, both experimental and computational evidence support a more concerted H atom transfer in the present system. The DFT-calculated BDE for the DHP N-H bond of 56 kcal/mol is comparatively small and thus energetically accessible for a HAT pathway (Table S14). Inspection of the Mulliken charges along the reaction coordinate also suggests that each transition state is best described as an H atom (H+ + e-) transfer rather than a heterolytic proton and hydride transfer (Table S15). Thus, while both of these Ni-based electrocatalysts rely on hydridefree mechanisms, the present DHP system leverages ligandbased interactions to specifically shuttle H atom equivalents to the bound alkyne substrate as opposed to more purely outersphere steps in the bipyridine system.

CONCLUSIONS

We describe a homogeneous electrocatalytic system for the semihydrogenation of terminal alkynes and corresponding mechanistic investigations which support a ligand-assisted mechanism and Z-selective hydrogenation. The (fbu,TolDHP)Ni complex catalyzes selective semihydrogenation of a variety of alkyne substrates including those with alcohol, thiophene, pyridine, cyclopropyl, and chloride functional groups. The selective semihydrogenation of terminal alkynes without significant oligomerization or overreduction is unusual generally, and particularly so for an electrochemical system.

Mechanistic investigations support the importance of HAT from ligand-stored H atom equivalents to Ni-coordinated alkyne substrates. In our proposed catalytic pathway, the ligand and metal center work in tandem to selectively shuttle protons and electrons in a coordinated manner. While most examples of hydrogenation catalysts employ a metal hydride mechanism, this DHP system is unique in its involvement in ligand-based H atom storage, drawing inspiration from enzymatic processes. This catalytic design strategy, particularly that employed in reductive electrocatalysis here, opens new possibilities for selective and efficient transformations. Specifically, the use of electrochemical hydrogenation schemes enables fine-tuning of parameters including applied current, potential, and acid pK_a , offering possibly more delicate control compared to chemical redox conditions. The utility of the DHP scaffold in avoiding a competitive HER offers promise for general application in various reductive processes that more typically rely upon H₂.

■ EXPERIMENTAL SECTION

General Considerations. All reagents were purchased from commercial suppliers and used without further purification, unless otherwise specified. Complex 1 was synthesized following a previously reported procedure.⁵⁹ All manipulations were carried out under an atmosphere of N₂ by using standard Schlenk and glovebox techniques. Glassware was dried at 180 °C for a minimum of 2 h and cooled under vacuum prior to use. Solvents were dried on a solvent purification system from Pure Process Technology, passed over a column of activated alumina, and stored over 4 Å molecular sieves under N2. Tetrahydrofuran was stirred over NaK alloy and run through an additional activated alumina column prior to use to ensure dryness. C₆D₆ and CD₃CN were stored over 4 Å molecular sieves under N2. Solvents were tested for H2O and O2 using a standard solution of the sodium-benzophenone ketyl radical anion. Tetrabutylammonium hexafluorophosphate and benzoic acid were dried under vacuum at 100 °C over 8 h.

¹H and ¹³C NMR spectra were recorded on a Bruker DRX 400 MHz spectrometer. Chemical shifts are reported in parts per million units referenced to residual solvent resonances for ¹H spectra. Infrared spectra were recorded using a Bruker Tensor II spectrometer with OPUS software suite. IR samples were prepared using a solution cell with KBr windows. EPR spectra were recorded on an Elexsys E500 spectrometer with an Oxford ESR 900 X-band cryostat and a Bruker Cold-Edge Stinger and were simulated using the Easyspin suite in Matlab software.⁷⁴ GC/MS data was collected on an Agilent SQ GCMS with 5977A single quad MS and 7890B GC. Elemental analysis was performed by Midwest Microlabs. Electrochemical measurements were performed using a BAS Epsilon potentiostat and analyzed using BAS Epsilon software version 1.40.67NT.

Electrochemical Experiments. Experiments were performed inside the glovebox with a MeCN/0.1 M nBu_4NPF_6 electrolyte solution at room temperature. Cyclic voltammetry measurements were made with a [Ni] = 1 mM using a glassy carbon working electrode, platinum wire counter electrode, and silver wire pseudoreference electrode and were referenced to internal Fc/Fc⁺ by adding ferrocene at the end of measurements. A one-compartment

glass cell was filled with 4 mL of electrolyte solution. The working electrode was polished over a microcloth pad (Buehler) using alumina slurry (0.05 mm EMS), followed by rinsing with deionized water and isopropyl alcohol. Reference and counter electrodes were rinsed with acetone. CVs were recorded at a scan rate of 100 mV/s scanning reductively.

Electrolyses were performed in an H-type glass cell with anode and cathode chambers separated by a glass frit. An RVC (reticulated vitreous carbon, ERG Duocel, 2 cm × 0.5 cm x 0.5 cm) electrode, Zn rod (National Bureau of Standards, 3 cm × 0.5 cm x 0.5 cm), and a AgBF₄/Ag electrode (BASi, 0.05 mm, 10 mM AgBF₄ solution in MeCN 0.1 M nBu₄NPF₆) were used as working, counter, and reference electrodes, respectively. To each chamber of the H-cell was added 4 mL of electrolyte solution and stir bars. Typically, 2 mg of (DHP)Ni (final concentration of 1 mM), 100 mL of a mesitylene (internal standard) solution in MeCN (final concentration of 10 mM), 100 mL of a substrate solution in MeCN (final concentration of 10 mM), and benzoic acid (final concentration of 1 M) were added to the cathodic chamber. Electrolyses were performed under galvanostatic conditions, and aliquots were taken and diluted in MeCN before analysis by gas chromatography (GC). For determining the final in situ yield, the electrolyte solution was passed through an alumina pad, and 200 mL of CD₃CN was added to 200 mL of electrolyte solution and analyzed by ¹H NMR using a mesitylene internal standard (10 mM, δ 6.77 ppm, 3H) and a solvent suppression pulse sequence. All electrolytes were performed in triplicate. For substrates with <95% yield of the semihydrogenated product, GC-MS chromatograms and mass spectra are provided to check for the presence of alkene or dimerized products (see SI). Cyclopropylacetylene and methyl propiolate were too low-boiling to detect over-trace solvents by GC-MS on our instrument. Potentials reported for chronopotentiometry electrolysis experiments are referenced to Fc/ Fc+ by external measurement in an independent cell versus the $AgBF_4/Ag$ electrode of $E_{1/2}(Fc/Fc^+) = 0.48 \text{ V}$ vs $AgBF_4/Ag$. For electrolysis under an H2 atmosphere, the cathodic chamber was prepared in an N2 glovebox, removed from the glovebox, and sparged with H₂ for 10 min before starting electrolysis and then constantly during electrolysis.

X-ray Structure Determination. The diffraction data for 2 were measured at 100 K on a Bruker D8 fixed-chi with a PILATUS1M (CdTe) pixel array detector (synchrotron radiation, $\lambda = 0.41328 \text{ Å}$ (30 keV)) at the Chem-MatCARS 15-ID-B beamline at the Advanced Photon Source (Argonne National Laboratory). Data reduction and integration were performed with the Bruker APEX3 software package (Bruker AXS, version 2017.3-0, 2018). Data were scaled and corrected for absorption effects using the multiscan procedure as implemented in SADABS (Bruker AXS, version 2014/5).⁷⁵ The structures were solved by SHELXT (Version 2014/5)⁷⁶ and refined by a full-matrix least-squares procedure using OLEX2 (XL refinement program version 2018/1).77,78 Structure solutions were performed with the use of standard restraints and constraints as implemented in ShelXL. We note that the structure of 2 has A-level CheckCIF alerts arising from the fact that this data set was collected on a synchrotron, resulting in somewhat limited data completeness. Additional crystallographic and refinement data can be found in the SI.

Synthesis of ($^{18u,Tol}DHP$)Ni[CoCp₂*] (2). A solution of decamethyl-cobaltocene (CoCp₂*, 20 mg, 0.06 mmol) in THF (1 mL) was added all at once to a stirring solution of 1 (30 mg, 0.06 mmol) in THF (2 mL). After stirring at room temperature for 2 h, the color of the reaction mixture changed from deep violet to deep indigo. The solution was filtered, and the solvent was removed under vacuum, resulting in a deep indigo solid. The product was purified by recrystallization (concentrated THF, -35 °C). Yield: 44 mg, 0.053 mmol, 88%. ¹H NMR (400 MHz, C_6D_6): δ = 7.5 (d, 4H, J = 7.4 Hz), 7.08 (d, 4H, J = 7.0 Hz), 5.86 (s, 2H), 2.33 (s, 6H), 1.25 (s, 18H), 1.7 (s, 30H). ¹³C{¹H} NMR (125 MHz, C_6D_6): δ 141.7, 142.3, 138.1, 136.0, 129.3, 128.4, 111.5, 94.9, 52.7, 29.3, 20.9, 7.5. IR (ATR, cm⁻¹): 2954 (m), 2911 (m), 1511 (m, C=N), 1371 (m), 1341 (s), 1197 (m), 1103 (m), 1013 (s), 882 (w), 823 (s, C=C of CoCp₂*), 681 (m), 589 (m), 442 (m). Anal. calcd: C, 69.57; H, 7.78; N, 8.45;

found: C, 69.13; H, 7.57; N, 8.25. HRA-MS (m/z) [M]⁺ $C_{48}H_{64}N_5$ CoNi: 827.385 Found: 827.383.

Synthesis of ($^{18u,Tol}DHPH_2$)Ni($C_6H_5COO^-$) (3). To a stirring solution of 2 (10 mg, 0.012 mmol) at room temperature in a glovebox under a N_2 atmosphere in THF (300 mL) was added benzoic acid (2.9 mg, 0.024 mmol) dissolved in THF (300 mL). After stirring for 15 min, the solution was filtered, and the solvent was removed under vacuum. 1H NMR (400 MHz, C_6D_6 with a few drops of d_8 -THF for solubility): $\delta = 7.61$ (d, 4H, J = 7.3 Hz), 7.03 (d, 4H, J = 7.1 Hz), 6.66 (s, 2H), 5.92 (bs, 2H), 2.12 (s, 6H), 1.18 (s, 18H). IR (solution cell, THF, cm⁻¹): 3250 (b, N–H).

Chemical Reduction of 1-Octyne with 3 and Na/Hg. To a stirring solution of 3 (7.5 mg, 0.012 mmol) at room temperature in a glovebox under a $\rm N_2$ atmosphere in CD₃CN (600 mL) was added 1-octyne (17 μ L, 0.12 mmol) and Na amalgam (5% Na, 10 mg). After stirring for 30 min, the solution was filtered to remove the amalgam and transferred to an NMR tube to look for the presence of 1-octene by 1 H NMR. Mesitylene was used as an internal standard (1.7 μ L, 0.012 mmol). The control reaction was performed under the same conditions except for the absence of 3 in solution. See the Supporting Information.

Synthesis of d_1 -Benzoic Acid. Benzoic acid anhydride (Sigma-Aldrich, 1.0 g, 4.4 mmol) was stirred in D_2O (Cambridge Isotope, 99.9%, 10 mL) and refluxed under N_2 for 48 h. Upon cooling to room temperature, the product began to crystallize and could be collected by filtration as a white solid. The solid was further dried and purified by sublimation at 100 °C under reduced pressure before use. The 1H NMR spectrum is consistent with benzoic acid, with the absence of a broad OH peak usually found at 11.5 ppm. Comparison with the 1H NMR spectrum of benzoic acid anhydride shows that no starting material remains. See Figure S8 for the overlaid spectra.

Synthesis of 1-(Prop-2-yn-1-yloxy)hept-3-yne. To a stirred solution of 3-heptyn-1-ol (1.5 g, 13.4 mmol) in DMF (60 mL) was added K₂CO₃ (7.40 g, 53.6 mmol) in one portion. The resulting mixture was heated at 70 °C for 0.5 h, then 3-bromo-1-propyne (1.9 g, 16.1 mmol) dissolved in DMF (40 mL) was added slowly over 5 min. The mixture was heated at 70 °C for another 48 h. Upon completion, 15 mL of water was added. The mixture was extracted with Et₂O (3 × 100 mL). The combined organic layers were washed with water (4 × 100 mL) and brine (100 mL). After the removal of the solvent under reduced pressure, the resulting yellow oil was purified by flash chromatography on silica gel (hexanes/AcOEt: 95/ 5). Yield 96 mg (0.64 mmol, 5%). ¹H NMR (400 MHz, CDCl₃, RT): $\delta = 4.73$ (d, 2H, J = 2.4 Hz), 4.23 (t, 2H, J = 7.1 Hz), 2.55 (tt, 2H, J = 7.1 Hz), 2.55 (tt, 2H, J = 7.1 Hz) 2.4 Hz), 2.52 (t, 1H, J = 2.4 Hz), 2.11 (tt, 2H, J = 2.4 Hz), 1.50 (m, 2H, J = 7.2 Hz), 0.96 (t, 3H, J = 7.4 Hz). ¹³C { ¹H} NMR (125 MHz, $CDCl_3$, RT): $\delta = 154.4$, 82.4, 75.7, 74.8, 66.7, 55.3, 22.2, 20.7, 19.3,

Computational Methodology. Intermediates and transition states for the reaction coordinate with 1-butyne were optimized in ORCA⁷⁹ using the M06L functional and def2-TZVPP basis set on Ni, def2-TZVP basis set on all other atoms. Frequency calculations were performed to confirm that the structures are at local minima on the potential energy surface. The calculated BDE for the ligand NH's was determined using free energies from frequency calculations with the M06L functional and def2-TZVPP basis set for Ni and def2-TZVP for all other atoms. A simplified ligand with iPr groups in the place of the p-tol substituents was utilized as well as a 1-butyne substrate to reduce the number of atoms per calculation. We were unable to optimize geometry for TS1 as all TS calculations resulted in either falling off of the TS geometry to reactants or products or a lack of convergence. The proposed geometry for TS1 was obtained from a relaxed surface scan. (Figure S66) Frequency calculations of this geometry show two imaginary modes. The first corresponds to an N-H stretch for the productive reaction, and the second is a low magnitude (30 cm⁻¹) spurious ligand arm rotation. Thus, this geometry should be a reasonable estimate of the true TS geometry. This geometry for TS1 was further analyzed with an intrinsic reaction coordinate calculation (IRC) to verify it as a reasonable geometry (Figure S75). The IRC calculation was performed by using geometries along the optimized

transition state imaginary vibrational mode and calculating the forward and backward segments separately. The IRC calculations support the obtained geometry for TS1. The same functional and basis sets were used for all calculations.

ASSOCIATED CONTENT

Supporting Information

The Supporting Information is available free of charge at https://pubs.acs.org/doi/10.1021/jacs.3c09885.

Experimental procedures, NMR, GC/MS, electrochemistry, EPR, electrochemistry, SXRD data, and DFT (PDF)

Accession Codes

CCDC 2267244 contains the supplementary crystallographic data for this paper. These data can be obtained free of charge via www.ccdc.cam.ac.uk/data_request/cif, or by emailing data_request@ccdc.cam.ac.uk, or by contacting The Cambridge Crystallographic Data Centre, 12 Union Road, Cambridge CB2 1EZ, UK; fax: +44 1223 336033.

AUTHOR INFORMATION

Corresponding Author

John S. Anderson – Department of Chemistry, University of Chicago, Chicago, Illinois 60637, United States;

o orcid.org/0000-0002-0730-3018; Email: jsanderson@uchicago.edu

Authors

Maia E. Czaikowski – Department of Chemistry, University of Chicago, Chicago, Illinois 60637, United States;

© orcid.org/0000-0002-1334-8140

Sophie W. Anferov – Department of Chemistry, University of Chicago, Chicago, Illinois 60637, United States;

orcid.org/0000-0003-3972-5845

Alex P. Tascher – Department of Chemistry, University of Chicago, Chicago, Illinois 60637, United States

Complete contact information is available at: https://pubs.acs.org/10.1021/jacs.3c09885

Notes

The authors declare no competing financial interest.

ACKNOWLEDGMENTS

This work was supported by the National Institutes of Health (R35 GM133470) and as part of the Inorganometallic Catalysis Design Center, an Energy Frontier Research Center funded by the U.S. Department of Energy, Office of Science, Basic Energy Sciences (DE-SC0012702). We thank the University of Chicago for funding, and J.S.A. thanks the Dreyfus Foundation for a Teacher-Scholar Award (TC-21-064). We thank Joseph Schneider for assistance with EPR measurements and calculations. We also thank the Research Computing Cluster at the University of Chicago for providing computing resources. Some data reported here was collected at ChemMatCARS Sector 15 which is supported by the NSF under grant number NSF/CHE-1834750. This research used resources of the APS, a U.S. DOE Office of Science User Facility operated for the DOE Office of Science by Argonne National Laboratory under Contract No. DE-AC02-06CH11357. We would like to thank Dr.Yu-Sheng Chen for assistance with SXRD acquisition at 15-ID-B,C,D.

REFERENCES

- (1) Swamy, K. C. K.; Reddy, A. S.; Sandeep, K.; Kalyani, A. Advances in chemoselective and/or stereoselective semihydrogenation of alkynes. *Tetrahedron Lett.* **2018**, *59*, 419–429.
- (2) Decker, D.; Drexler, H.-J.; Heller, D.; Beweries, T. Homogeneous catalytic transfer semihydrogenation of alkynes an overview of hydrogen sources, catalysts and reaction mechanisms. *Catal. Sci. & Technol.* **2020**, *10*, 6449—6463.
- (3) Li, X.-T.; Chen, L.; Shang, C.; Liu, Z.-P. Selectivity control in alkyne semihydrogenation: Recent experimental and theoretical progress. *Chin. J. Catal.* **2022**, *43*, 1991–2000.
- (4) Lindlar, H. Ein neuer Katalysator für selektive Hydrierungen. Helv. Chim. Acta 1952, 35, 446–450.
- (5) Farrar-Tobar, R. A.; Weber, S.; Csendes, Z.; Ammaturo, A.; Fleissner, S.; Hoffmann, H.; Veiros, L. F.; Kirchner, K. E-Selective Manganese-Catalyzed Semihydrogenation of Alkynes with H2 Directly Employed or In Situ-Generated. *ACS Catal.* **2022**, *12*, 2253–2260.
- (6) Tokmic, K.; Fout, A. R. Alkyne Semihydrogenation with a Well-Defined Nonclassical Co–H2 Catalyst: A H2 Spin on Isomerization and E-Selectivity. *J. Am. Chem. Soc.* **2016**, *138*, 13700–13705.
- (7) Gorgas, N.; Brünig, J.; Stöger, B.; Vanicek, S.; Tilset, M.; Veiros, L. F.; Kirchner, K. Efficient Z-Selective Semihydrogenation of Internal Alkynes Catalyzed by Cationic Iron(II) Hydride Complexes. *J. Am. Chem. Soc.* **2019**, *141*, 17452–17458.
- (8) Hale, D. J.; Ferguson, M. J.; Turculet, L. (PSiP)Ni-Catalyzed (E)-Selective Semihydrogenation of Alkynes with Molecular Hydrogen. *ACS Catal.* **2022**, *12*, 146–155.
- (9) Kaicharla, T.; Zimmermann, B. M.; Oestreich, M.; Teichert, J. F. Using alcohols as simple H2-equivalents for copper-catalysed transfer semihydrogenations of alkynes. *Chem. Commun.* **2019**, *55*, 13410–13413.
- (10) Sansores-Paredes, M. L. G.; Lutz, M.; Moret, M.-E. Cooperative H2 activation at a nickel(0)—olefin centre. *Nat. Chem.* **2023**, DOI: 10.1038/s41557-023-01380-1.
- (11) Wang, S.; Uwakwe, K.; Yu, L.; Ye, J.; Zhu, Y.; Hu, J.; Chen, R.; Zhang, Z.; Zhou, Z.; Li, J.; Xie, Z.; Deng, D. Highly efficient ethylene production via electrocatalytic hydrogenation of acetylene under mild conditions. *Nature Commun.* **2021**, *12*, 7072.
- (12) Li, H.; Gao, Y.; Wu, Y.; Liu, C.; Cheng, C.; Chen, F.; Shi, Y.; Zhang, B. σ -Alkynyl Adsorption Enables Electrocatalytic Semi-hydrogenation of Terminal Alkynes with Easy-Reducible/Passivated Groups over Amorphous PdSx Nanocapsules. *J. Am. Chem. Soc.* **2022**, 144, 19456–19465.
- (13) Yan, M.; Kawamata, Y.; Baran, P. S. Synthetic Organic Electrochemical Methods Since 2000: On the Verge of a Renaissance. *Chem. Rev.* **2017**, *117*, 13230–13319.
- (14) Wiebe, A.; Gieshoff, T.; Möhle, S.; Rodrigo, E.; Zirbes, M.; Waldvogel, S. R. Electrifying Organic Synthesis. *Angew. Chem., Int. Ed.* **2018**, *57*, 5594–5619.
- (15) Jutand, A. Contribution of Electrochemistry to Organometallic Catalysis. *Chem. Rev.* **2008**, *108*, 2300–2347.
- (16) Francke, R.; Little, R. D. Redox catalysis in organic electrosynthesis: basic principles and recent developments. *Chem. Soc. Rev.* **2014**, *43*, 2492–2521.
- (17) IRENA. Renewable Power Generation Costs in 2020; International Renewable Energy Agency: Abu Dhabi, 2021.
- (18) Zhang, S.; Findlater, M. Electrochemically Driven Hydrogen Atom Transfer Catalysis: A Tool for C(sp3)/Si-H Functionalization and Hydrofunctionalization of Alkenes. *ACS Catal.* **2023**, *13*, 8731–8751.
- (19) Kaeffer, N.; Leitner, W. Electrocatalysis with Molecular Transition-Metal Complexes for Reductive Organic Synthesis. *JACS Au* **2022**, *2*, 1266–1289.
- (20) Du, P.; Mubarak, M. S.; Karty, J. A.; Peters, D. G. Electrosynthesis of 4-Methylcoumarin via Cobalt(I)-Catalyzed Reduction of 2-Acetylphenyl 2-Chloroacetate or 2-Acetylphenyl 2,2-Dichloroacetate. *J. Electrochem. Soc.* **2007**, *154*, F231.

- (21) Raess, P. W.; Mubarak, M. S.; Ischay, M. A.; Foley, M. P.; Jennermann, T. B.; Raghavachari, K.; Peters, D. G. Catalytic reduction of 1-iodooctane by nickel(I) salen electrogenerated at carbon cathodes in dimethylformamide: Effects of added proton donors and a mechanism involving both metal- and ligand-centered one-electron reduction of nickel(II) salen. *J. Electroanal. Chem.* **2007**, 603, 124–134
- (22) Mubarak, M. S.; Jennermann, T. B.; Ischay, M. A.; Peters, D. G. Catalytic Reduction of Phenyl-Conjugated Acetylenic Halides by Nickel(I) Salen: Cyclization versus Coupling. *Eur. J. Org. Chem.* **2007**, 2007, 5346–5352.
- (23) Miranda, J. A.; Wade, C. J.; Little, R. D. Indirect Electroreductive Cyclization and Electrohydrocyclization Using Catalytic Reduced Nickel(II) Salen. *J. Org. Chem.* **2005**, *70*, 8017–8026.
- (24) Fokin, I.; Kuessner, K.-T.; Siewert, I. Electroreduction of Carbonyl Compounds Catalyzed by a Manganese Complex. *ACS Catal.* **2022**, *12*, 8632–8640.
- (25) Derosa, J.; Garrido-Barros, P.; Peters, J. C. Electrocatalytic Reduction of C–C π -Bonds via a Cobaltocene-Derived Concerted Proton–Electron Transfer Mediator: Fumarate Hydrogenation as a Model Study. *J. Am. Chem. Soc.* **2021**, *143*, 9303–9307.
- (26) Schendzielorz, F.; Finger, M.; Abbenseth, J.; Würtele, C.; Krewald, V.; Schneider, S. Metal-Ligand Cooperative Synthesis of Benzonitrile by Electrochemical Reduction and Photolytic Splitting of Dinitrogen. *Angew. Chem., Int. Ed.* **2019**, *58*, 830–834.
- (27) van der Meer, M.; Rechkemmer, Y.; Peremykin, I.; Hohloch, S.; van Slageren, J.; Sarkar, B. (Electro)catalytic C–C bond formation reaction with a redox-active cobalt complex. *Chem. Commun.* **2014**, *50*, 11104–11106.
- (28) Wuttig, A.; Derrick, J. S.; Loipersberger, M.; Snider, A.; Head-Gordon, M.; Chang, C. J.; Toste, F. D. Controlled Single-Electron Transfer via Metal—Ligand Cooperativity Drives Divergent Nickel-Electrocatalyzed Radical Pathways. *J. Am. Chem. Soc.* **2021**, *143*, 6990—7001.
- (29) Gnaim, S.; Bauer, A.; Zhang, H.-J.; Chen, L.; Gannett, C.; Malapit, C. A.; Hill, D. E.; Vogt, D.; Tang, T.; Daley, R. A.; Hao, W.; Zeng, R.; Quertenmont, M.; Beck, W. D.; Kandahari, E.; Vantourout, J. C.; Echeverria, P.-G.; Abruna, H. D.; Blackmond, D. G.; Minteer, S. D.; Reisman, S. E.; Sigman, M. S.; Baran, P. S. Cobalt-electrocatalytic HAT for functionalization of unsaturated C–C bonds. *Nature* **2022**, 605, 687–695.
- (30) Lee, M.-Y.; Kahl, C.; Kaeffer, N.; Leitner, W. Electrocatalytic Semihydrogenation of Alkynes with [Ni(bpy)3]2+. *JACS Au* **2022**, *2*, 573–578.
- (31) Hydride- Durin, G.; Lee, M.-Y.; Pogany, M. A.; Weyhermüller, T.; Kaeffer, N.; Leitner, W. Free Hydrogenation: Unraveling the Mechanism of Electrocatalytic Alkyne Semihydrogenation by Nickel–Bipyridine Complexes. *J. Am. Chem. Soc.* **2023**, *145*, 17103–17111.
- (32) Anferov, S. W.; Filatov, A. S.; Anderson, J. S. Cobalt-Catalyzed Hydrogenation Reactions Enabled by Ligand-Based Storage of Dihydrogen. ACS Catal. 2022, 12, 9933–9943.
- (33) Käß, M.; Friedrich, A.; Drees, M.; Schneider, S. Ruthenium Complexes with Cooperative PNP Ligands: Bifunctional Catalysts for the Dehydrogenation of Ammonia–Borane. *Angew. Chem., Int. Ed.* **2009**, *48*, 905–907.
- (34) Khaskin, E.; Iron, M. A.; Shimon, L. J. W.; Zhang, J.; Milstein, D. N— H activation of amines and ammonia by Ru via metal—ligand cooperation. *J. Am. Chem. Soc.* **2010**, *132*, 8542.
- (35) Feller, M.; Diskin-Posner, Y.; Shimon, L. J. W.; Ben-Ari, E.; Milstein, D. N–H Activation by Rh (I) via Metal–Ligand Cooperation. *Organometallics* **2012**, *31*, 4083.
- (36) He, L. P.; Chen, T.; Gong, D.; Lai, Z.; Huang, K. W. Enhanced reactivities toward amines by introducing an imine arm to the pincer ligand: direct coupling of two amines to form an imine without oxidant. *Organometallics* **2012**, *31*, 5208.
- (37) Rodríguez-Lugo, R. E.; Trincado, M.; Vogt, M.; Tewes, F.; Santiso-Quinones, G.; Grützmacher, H. A homogeneous transition metal complex for clean hydrogen production from methanol—water mixtures. *Nat. Chem.* **2013**, *5*, 342–347.

- (38) Myers, T. W.; Berben, L. A. Aluminum—ligand cooperative N—H bond activation and an example of dehydrogenative coupling. *J. Am. Chem. Soc.* **2013**, *135*, 9988—9990.
- (39) Xu, R.; Chakraborty, S.; Bellows, S. M.; Yuan, H.; Cundari, T. R.; Jones, W. D. Iron-Catalyzed Homogeneous Hydrogenation of Alkenes under Mild Conditions by a Stepwise, Bifunctional Mechanism. *ACS Catal.* **2016**, *6*, 2127–2135.
- (40) Sherbow, T. J.; Fettinger, J. C.; Berben, L. A. Control of Ligand pKa Values Tunes the Electrocatalytic Dihydrogen Evolution Mechanism in a Redox-Active Aluminum(III) Complex. *Inorg. Chem.* **2017**, *56*, 8651–8660.
- (41) Rajabimoghadam, K.; Darwish, Y.; Bashir, Y.; Pirman, D.; Eichelberger, S.; Sieler, M. A.; Swart, M.; Garcia-Bosch, I. Catalytic aerobic oxidation of alcohols by copper complexes bearing redoxactive ligands with tunable H-bonding groups. *J. Am. Chem. Soc.* **2018**, 140, 16625–16634.
- (42) Sinha, S.; Das, S.; Mondal, R.; Mandal, S.; Paul, N. D. Cobalt complexes of redox noninnocent azo-aromatic pincers. Isolation, characterization, and application as catalysts for the synthesis of quinazolin-4 (3 H)-ones. *Dalton Trans.* **2020**, *49*, 8448–8459.
- (43) Thompson, E. J.; Berben, L. A. Electrocatalytic Hydrogen Production by an Aluminum (III) Complex: Ligand-Based Proton and Electron Transfer. *Angew. Chem., Int. Ed.* **2015**, *54*, 11642–11646.
- (44) Margulieux, G. W.; Bezdek, M. J.; Turner, Z. R.; Chirik, P. J. Ammonia Activation, H2 Evolution and Nitride Formation from a Molybdenum Complex with a Chemically and Redox Noninnocent Ligand. *J. Am. Chem. Soc.* **2017**, *139*, 6110–6113.
- (45) Dauth, A.; Gellrich, U.; Diskin-Posner, Y.; Ben-David, Y.; Milstein, D. The ferraquinone—ferrahydroquinone couple: combining quinonic and metal-based reactivity. *J. Am. Chem. Soc.* **2017**, *139*, 2799–2807.
- (46) Rosenkoetter, K. E.; Wojnar, M. K.; Charette, B. J.; Ziller, J. W.; Heyduk, A. F. Hydrogen-atom noninnocence of a tridentate [SNS] pincer ligand. *Inorg. Chem.* **2018**, *57*, 9728–9737.
- (47) Ward, M. B.; Scheitler, A.; Yu, M.; Senft, L.; Zillmann, A. S.; Gorden, J. D.; Schwartz, D. D.; Ivanović-Burmazović, D. D.; Goldsmith, C. R. Superoxide dismutase activity enabled by a redoxactive ligand rather than metal. *Nat. Chem.* **2018**, *10*, 1207–1212.
- (48) Drummond, M. J.; Ford, C. L.; Gray, D. L.; Popescu, C. V.; Fout, A. R. Radical Rebound Hydroxylation Versus H-Atom Transfer in Non-Heme Iron(III)-Hydroxo Complexes: Reactivity and Structural Differentiation. *J. Am. Chem. Soc.* **2019**, *141*, 6639–6650.
- (49) Purse, B. W.; Tran, L.-H.; Piera, J.; Åkermark, B.; Bäckvall, J.-E. Synthesis of New Hybrid Hydroquinone/Cobalt Schiff Base Catalysts: Efficient Electron-Transfer Mediators in Aerobic Oxidation. *Chem. Eur. J.* **2008**, *14*, 7500–7503.
- (50) Myers, T. W.; Berben, L. A. Aluminium–ligand cooperation promotes selective dehydrogenation of formic acid to H2 and CO2. *Chem. Sci.* **2014**, *5*, 2771–2777.
- (51) Henthorn, J. T.; Lin, S.; Agapie, T. Combination of Redox-Active Ligand and Lewis Acid for Dioxygen Reduction with π-Bound Molybdenum— Quinonoid Complexes. J. Am. Chem. Soc. 2015, 137, 1458–1464.
- (52) Lagaditis, P. O.; Schluschaß, B.; Demeshko, S.; Würtele, C.; Schneider, S. Square-Planar Cobalt (III) Pincer Complex. *Inorg. Chem.* **2016**, *55*, 4529–4536.
- (53) Schneck, F.; Finger, M.; Tromp, M.; Schneider, S. Chemical Non-Innocence of an Aliphatic PNP Pincer Ligand. *Chem. Eur. J.* **2017**, 23, 33–37.
- (54) Lindley, B. M.; Bruch, Q. J.; White, P. S.; Hasanayn, F.; Miller, A. J. M. Ammonia Synthesis from a Pincer Ruthenium Nitride via Metal—Ligand Cooperative Proton-Coupled Electron Transfer. *J. Am. Chem. Soc.* **2017**, *139*, 5305–5308.
- (55) Pramanick, R.; Bhattacharjee, R.; Sengupta, D.; Datta, A.; Goswami, S. An azoaromatic ligand as four electron four proton reservoir: catalytic dehydrogenation of alcohols by its zinc (II) complex. *Inorg. Chem.* **2018**, *57*, 6816–6824.

- (56) Jain, R.; Mamun, A. A.; Buchanan, R. M.; Kozlowski, P. M.; Grapperhaus, C. A. Ligand-assisted metal-centered electrocatalytic hydrogen evolution upon reduction of a bis (thiosemicarbazonato) Ni (II) complex. *Inorg. Chem.* **2018**, *57*, 13486–13493.
- (57) Sherbow, T. J.; Thompson, E. J.; Arnold, A.; Sayler, R. I.; Britt, R. D.; Berben, L. A. Electrochemical Reduction of N2 to NH3 at Low Potential by a Molecular Aluminum Complex. *Chem. Eur. J.* **2019**, 25, 454–458.
- (58) McNeece, A. J.; Jesse, K. A.; Filatov, A. S.; Schneider, J. E.; Anderson, J. S. Catalytic hydrogenation enabled by ligand-based storage of hydrogen. *Chem. Commun.* **2021**, *57*, 3869–3872.
- (59) McNeece, A. J.; Jesse, K. A.; Xie, J.; Filatov, A. S.; Anderson, J. S. Generation and Oxidative Reactivity of a Ni(II) Superoxo Complex via Ligand-Based Redox Non-Innocence. *J. Am. Chem. Soc.* **2020**, *142*, 10824–10832.
- (60) Beyene, B. B.; Hung, C.-H. Recent progress on metalloporphyrin-based hydrogen evolution catalysis. *Coord. Chem. Rev.* **2020**, *410*, No. 213234.
- (61) Canaguier, S.; Artero, V.; Fontecave, M. Modelling NiFe hydrogenases: nickel-based electrocatalysts for hydrogen production. *Dalton Trans.* **2008**, 315–325.
- (62) Dressel, J. M.; Cook, E. N.; Hooe, S. L.; Moreno, J. J.; Dickie, D. A.; Machan, C. W. Electrocatalytic hydrogen evolution reaction by a $Ni(N_2O_2)$ complex based on 2,2'-bipyridine. *Inorg. Chem. Front.* **2023**, *10*, 972–978.
- (63) Fang, M.; Engelhard, M. H.; Zhu, Z.; Helm, M. L.; Roberts, J. A. S. Electrodeposition from acidic solutions of Nickel bis-(benzenedithiolate) produces a hydrogen evolving Ni-S film on glassy carbon. *ACS Catal.* **2014**, *4*, 90–98.
- (64) Han, Z.; Shen, L.; Brennessel, W. W.; Holland, P. L.; Eisenberg, R. Nickel Pyridinethiolate Complexes as Catalysts for the Light-Driven Production of Hydrogen from Aqueous Solutions in Noble-Metal-Free Systems. *J. Am. Chem. Soc.* **2013**, *135*, 14659–14669.
- (65) Helm, M. L.; Stewart, M. P.; Bullock, R. M.; DuBois, M. R.; DuBois, D. L. A Synthetic Nickel Electrocatalyst with a Turnover Frequency Above $100,000~\rm s^{-1}$ for $\rm H_2$ Production. *Science* **2011**, 333, 863–866.
- (66) Jacques, P.; Artero, V.; Pecaut, J.; Fontecave, M. Cobalt and nickel diimine-dioxime complexes as molecular electrocatalysts for hydrogen evolution with low overvoltages. *Proc. Natl. Acad. Sci. U. S. A.* **2009**, *106*, 20627–20632.
- (67) Khrizanforova, V. V.; Fayzullin, R. R.; Musina, E. I.; Karasik, A. A.; Budnikova, Y. H. Electrochemical and catalytic properties of nickel(II) complexes with bis(imino)acenaphthene and diazadiphosphacyclooctane ligands. *Mendeleev Commun.* **2020**, *30*, 302–304.
- (68) Martin, D. J.; McCarthy, B. D.; Donley, C. L.; Dempsey, J. L. Electrochemical hydrogenation of a homogeneous nickel complex to form a surface adsorbed hydrogen-evolving species. *Chem. Commun.* **2015**, *51*, 5290–5293.
- (69) Pantani, O.; Anxolabéhère-Mallart, E.; Aukauloo, A.; Millet, P. Electroactivity of cobalt and nickel glyoximes with regard to the electro-reduction of protons into molecular hydrogen in acidic media. *Electrochem. Commun.* **2007**, *9*, 54–58.
- (70) Rao, H.; Yu, W.-Q.; Zheng, H.-Q.; Bonin, J.; Fan, Y.-T.; Hou, H.-W. Highly efficient photocatalytic hydrogen evolution from nickel quinolinethiolate complexes under visible light irradiation. *J. Power Sources* **2016**, 324, 253–260.
- (71) Shotonwa, I. O.; Ejeromedoghene, O.; Adesoji, A. O.; Adewuyi, S. Electrochemistry and electrocatalysis of H2 generation using hexacoordinated nickel—based complexes. *Catal. Comm.* **2023**, *179*, No. 106680.
- (72) Rountree, E. S.; McCarthy, B. D.; Eisenhart, T. T.; Dempsey, J. L. Evaluation of Homogeneous Electrocatalysts by Cyclic Voltammetry. *Inorg. Chem.* **2014**, *53*, 9983–10002.
- (73) Newcomb, M. Radical Kinetics and Clocks. In *Encyclopedia of Radicals in Chemistry, Biology and Materials*; John Wiley & Sons, 2012. (74) Stoll, S.; Schweiger, A. EasySpin, a comprehensive software package for spectral simulation and analysis in EPR. *J. Magn. Reson.* **2006**, 178, 42–55.

- (75) Krause, L.; Herbst-Irmer, R.; Sheldrick, G. M.; Stalke, D. Comparison of Silver and Molybdenum Microfocus X-Ray Sources for Single-Crystal Structure Determination. *J. Appl. Crystallogr.* **2015**, 48, 3–10.
- (76) Sheldrick, G. M. SHELXT Integrated Space-Group and Crystal-Structure Determination. *Acta Crystallogr., Sect. A: Found. Adv.* **2015**, *71*, 3–8.
- (77) Dolomanov, O. V.; Bourhis, L. J.; Gildea, R. J.; Howard, J. A. K.; Puschmann, H. OLEX2: A Complete Structure Solution, Refinement and Analysis Program. *J. Appl. Crystallogr.* **2009**, *42*, 339–341.
- (78) Sheldrick, G. M. Crystal Structure Refinement with SHELXL. Acta Crystallogr., Sect. C. Struct. Chem. 2015, 71, 3–8.
- (79) Neese, F. The ORCA program system. WIREs Comput. Mol. Sci. 2012, 2, 73–78.